Smart Manufacturing and Material Processing (SMMP)

DOI: http://doi.org/10.26480/smmp.01.2023.59.65

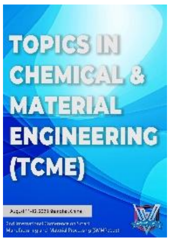

REVIEW ARTICLE

CONSTRUCTION AND PERFORMANCE RESEARCH OF VARIABLE CROSS-SECTION SCROLL PROFILE USING THE BASE CIRCLE INVOLUTE

Caisheng Hou[a,*], Yu Liu[a], Jinhu Li[a], Haroon Rasheed[b]

[a]*School of Mechanical Engineering, Ningxia University, Yinchuan, China*
[b]*Department of Civil Engineering, The Islamia University Bahawalpur, Pakistan*
[*]*Corresponding Author Email: houcs2019@163.com*

ARTICLE DETAILS

Article History:

Received 05 January 2024
Revised 08 February 2024
Accepted 11 March 2024
Available online 14 March 2024

ABSTRACT

The use of variable cross-section scroll profile is one of the effective ways to improve the performance of the scroll compressor. However, the existing variable cross-section scroll profiles have many disadvantages, such as difficult processing and unstable performance. For this reason, this paper adopted the base circle involute with stable performance and easy processing characteristics to construct a new type of variable cross-section scroll profile, and established the basic geometric theory of the profile. At the same time, two important indexes of volumetric performance, namely compression ratio and radial leakage line length, and a key index of mechanical performance, that is axial gas force, were introduced to evaluate its performance quantitatively. The results show that under the same basic parameters, compared with the equal cross-section profile formed by a single base circle involute as well as the traditional variable cross-section profile formed by the base circle involute, higher-order curve and base circle involute or circular arc, the volumetric performance and mechanical performance of the newly constructed variable cross-section profile are more advantageous, the compression ratio increased by 28.62%, 16.51% and 7.58% respectively; The length of radial leakage line is shortened by 26.56%, 16.37% and 14.23% respectively; The axial gas force is also significantly reduced, especially for the profile without the introduction of higher-order curve, the change range of the axial gas force is obviously smaller. The research broadens the design concept of the scroll profile, enriches the types of existing variable cross-section scroll profiles, and provides a certain theoretical basis for improving the performances of the scroll compressor.

KEYWORDS

Scroll compressor, base circle involute, variable cross-section scroll profile, volumetric performance, axial gas force

1. INTRODUCTION

The scroll compressor, which operates on the principle of conjugate profile meshing and chamber volume changing, has been widely valued for its advantages of high efficiency, energy conservation, low vibration and noise, compact structure, and high reliability since its inception. Currently, its applications in industries, medical treatment, refrigeration, and booster pumps have become increasingly mature (Qiu et al., 2018; Ivlev and Misyurin, 2017; Cavazzini et al., 2020; Diniz et al., 2015). In recent years, the research on scroll compressors has been in full swing, demonstrating excellent performance in waste heat recovery, cold chain transportation, and new energy vehicles.

The scroll profile is the key and basis for the design and development of scroll compressors. The curves that can be used as scroll profiles include base circle involute, positive polygon involute, line segment involute and variable diameter base circle involute, etc. Among these curves, the base circle involute is more widely used, mainly because of its many advantages in terms of performance, deformation and processing (Ahmad et al., 2020; Pereira and Deschamps, 2020; Zhen et al., 2022). For example, Wang et al proved that the scroll compressor consist of base circle involute has the lowest vibration and energy loss and the best performance through their research on the geometric characteristics and coupling mechanism dynamics of scroll profiles (Licun et al., 2009). Qiang et al. analyzed the geometric model and deformation characteristics of the scroll compression chamber, and concluded that the compression chamber composed of the base circle involute has stable deformation, high efficiency and relatively easy processing (Jianguo and Zhen Quan, 2009). Fan et al. proved from the perspective of the sensitivity of the rotation error of scroll profiles that the base circle involute is a profile with good error stability and has good robustness (Ling et al., 2023).

Although the base circle involute has many advantages mentioned above, it also has shortcomings such as small compression ratio and large leakage. If the compression ratio is to be increased, the number of circles of the scroll profiles should be increased, which in turn will cause an increase in the length of the leakage line. To overcome the above shortcomings, relevant scholars have proposed the idea of using combining curves to construct variable cross-section scroll profiles, thereby achieving the requirement of high compression ratio with fewer circles of profiles (Rak and Pietrowicz, 2020; Jiahao et al., 2022; Shuai et al., 2023).

However, when constructing variable cross-section profiles, it is inevitable to introduce higher-order curves, which can lead to the following defects in the variable cross-section profile. Firstly, changes in the length of the compression chamber and the integrated radius of curvature at the point of engagement can be very complex. Secondly, the processing difficulty and cost of the profile are high. Finally, when the design requirements of the profile change, it is easy to cause the profile to fail to connect smoothly at

Quick Response Code	Access this article online	
	Website: Website: www.topicsonchemeng.org.my	**DOI:** 10.26480/smmp.01.2023.59.65

Cite The Article: Caisheng Hou, Yu Liu, Jinhu Li, Haroon Rasheed (2023). Construction And Performance Research of Variable Cross-Section Scroll Profile Using The Base Circle Involute. *Topics In Chemical & Material Engineering, 2(1): 59-65.*

the connection point (Caisheng et al., 2021). Therefore, how to improve the compression ratio and shorten the length of the leakage line without using higher-order curves has become an urgent problem to be solved.

In view of this, based on the theory of differential geometry, this paper proposes to use the theory of base circle involute scroll profile to construct a new type of variable cross-section scroll profile. This profile not only takes into account the advantages of both the base circle involute and the variable cross-section profile, but also overcomes the drawbacks of introducing higher-order curves using traditional variable cross-section profiles.

2. Basic Geometric Theory

2.1 Differential Geometry Relation of base Circle Involute

As shown in Figure 1, it is a schematic diagram of the geometric relationship of the base circle involute. P is any point on the involute, φ is the tangential angle, R_s is the unfolding string, and R_g is the radius of the base circle, and meet the following requirements.

$$\frac{dR_s}{d\varphi} = R_g \tag{1}$$

Based on the above relationship, the equation for the scroll profile with respect to the tangential angle φ can be obtained by

$$\begin{cases} x = R_g \cos\varphi + R_s \sin\varphi \\ y = R_g \sin\varphi - R_s \cos\varphi \end{cases} \varphi \in [0, \varphi_{max} \tag{2}$$

Where φ_{max} is the maximum tangential angle of the scroll profile.

In order to construct a new type of variable-section scroll profiles using the base circle involute, dividing the scroll profile consisting of a single base circle involute into three segments, namely AC, CD and DH, denoted by S_1, S_2 and S_3respectively. To reduce the number of circles of the base circle involuteS_2, a new section of base circle involuteS_{2*} is introduced to replaceS_2， as shown in Figure 2(a).In section AC, the tangential angle range of the profile is $[0, \varphi_1)$, in section CD, the tangential angle range of the profile is $[\varphi_1, \varphi_1 + 2n_1\pi)$, in section DH, the tangential angle range of the profile is $[\varphi_1 + 2n_1\pi, \varphi_{max}$.

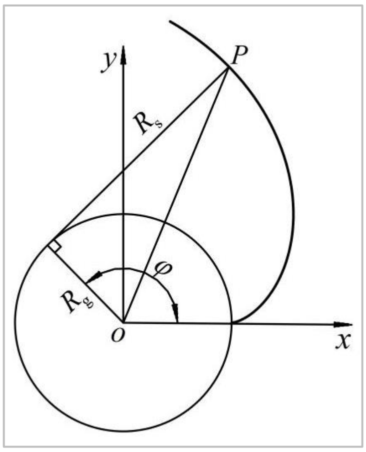

Figure 1: Geometric relationship of the base circle involute

According to above equations, the profile equations of the base circle involutes S_2 and S_{2*} can be obtained as follows

$$\begin{cases} x_2 = a\cos\varphi + a\varphi\sin\varphi \\ y_2 = a\sin\varphi - a\varphi\cos\varphi \end{cases} \varphi \in [\varphi_1, \varphi_1 + 2n_1\pi] \tag{3}$$

$$\begin{cases} x_2^* = a^*\cos\varphi^* + a^*\varphi^*\sin\varphi^* \\ y_2^* = a^*\sin\varphi^* - a^*\varphi^*\cos\varphi^* \end{cases} \varphi^* \in [\varphi_1^*, \varphi_1^* + 2n_2\pi] \tag{4}$$

Where a and n_1 are the base circle radius and number of circles of S_2, respectively; a^* and n_2 are the base circle radius and number of circles of S_{2*}, respectively, and satisfy $n_1 > n_2$.

When the base circle involuteS_2 lies at the two endpoints of the interval $[\varphi_1, \varphi_1 + 2n_1\pi]$, the coordinate points are noted as $C$and Drespectively, when the base circle involuteS_{2*}lies at the two endpoints of the interval $[\varphi_2, \varphi_2 + 2n_2\pi]$, the coordinate points are noted as E and F respectively, the base circle involutes S_2 and S_{2*} are the S_{CD} and S_{EF} in Figure 2 (a).

According to the plane curve theory in differential geometry, to make the base circle involute S_{2*} with circle number n_2 replace the base circle involute S_2 with circle number n_1, the distance between point C and point D must be equal to the distance between point E and point F, namely

$$l_{\mathrm{CD}} = l_{\mathrm{EF}} \tag{5}$$

Through above equation, the relationship between the radius of the base circle and the number of circles can be obtained as

$$\mathrm{a}n_1 = a^* n_2 \tag{6}$$

Rotate the involute S_{2*} of the base circle counterclockwise around the center of the base circle $\varphi_1 - \varphi_2$ to obtain $S_{E'F'}$, as shown in Figure 2 (b). From the figure, it can be seen that points $E^{'}$ and F' do not completely coincide with points C and D. Therefore, it is necessary to shift the profile $S_{E'F'}$ by a certain distance to make it completely coincide. The distance of translation is the distance between point C and point $E^{'}$, which can be expressed as

$$\begin{cases} \Delta x = (a^* - a)\cos\varphi_1 + (a^*\varphi_1^* - a\varphi_1)\sin\varphi_1 \\ \Delta y = (a^* - a)\sin\varphi_1 - (a^*\varphi_1^* - a\varphi_1)\cos\varphi_1 \end{cases} \tag{7}$$

After translation, point C and point E'' coincide completely, and point D and point $F^{''}$ also coincide completely, at which point $S_{E''F''}$ can completely replace S_2, as shown in Figure 2(c).

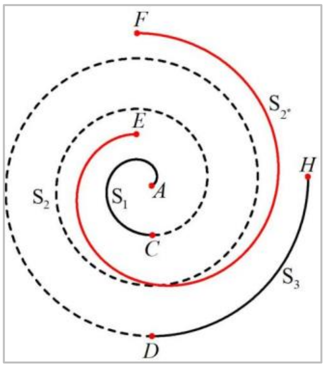

(a)

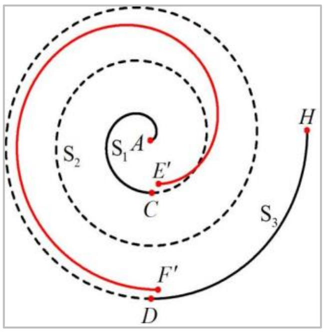

(b)

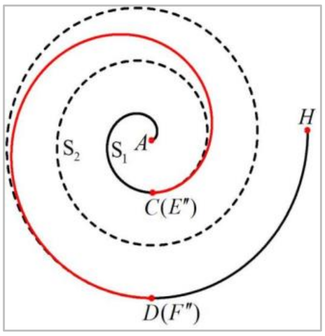

(c)

Figure 2: Variation diagram of the base circle involute

2.2 Construction of the Variable Cross Section Scroll Profile

To ensure a smooth transition of the newly constructed variable section scroll profile at the connection points C and D, the following transformations must be made to the base circle involutes $S_{E''F''}$ and S_3. Firstly, rotate the profile $S_{E''F''}$ counterclockwise around the point C by an angle ψ_1. Secondly, rotate the profile S_3 counterclockwise around the point C by an angle ψ_1, and finally rotate counterclockwise around point D by an angle ψ_2, the baseline equation of each segment of the variable section scroll profile can be obtained respectively.

The baseline equation for the involute of the first base circle can be given by:

$$\begin{cases} x_1 = a\cos\varphi + a\varphi\sin\varphi \\ y_1 = a\sin\varphi - a\varphi\cos\varphi \end{cases} \varphi \in [0, \varphi_1) \tag{8}$$

The baseline equation for the involute of the second base circle can be calculated by:

$$\begin{cases} x_2 = a^*\cos(\varphi+\psi_1) + a^*(\varphi-\varphi_1+\varphi_1^*)\sin(\varphi+\psi_1) - (a^*-a)\cos(\varphi_1+\psi_1) - (a^*\varphi_1^*-a\varphi_1)\sin(\varphi_1+\psi_1) - b_1\cos\psi_1 + c_1\sin\psi_1 + b_1 \\ y_2 = a^*\sin(\varphi+\psi_1) - a^*(\varphi-\varphi_1+\varphi_1^*)\cos(\varphi+\psi_1) - (a^*-a)\sin(\varphi_1+\psi_1) + (a^*\varphi_1^*-a\varphi_1)\cos(\varphi_1+\psi_1) - c_1\cos\psi_1 - b_1\sin\psi_1 + c_1 \end{cases} \varphi \in [\varphi_1, \varphi_1 + 2n_2\pi] \tag{9}$$

The baseline equation for the involute of the third base circle can be expressed as:

$$\begin{cases} x_3 = a\cos(\varphi+\psi_1+\psi_2) + a\varphi\sin(\varphi+\psi_1+\psi_2) - b_1\cos(\psi_1+\psi_2) + c_1\sin(\psi_1+\psi_2) + (b_1-b_2)\cos\psi_2 - (c_1-c_2)\sin\psi_2 + b_2 \\ y_3 = a\sin(\varphi+\psi_1+\psi_2) - a\varphi\cos(\varphi+\psi_1+\psi_2) - b_1\sin(\psi_1+\psi_2) - c_1\cos(\psi_1+\psi_2) + (b_1-b_2)\sin\psi_2 + (c_1-c_2)\cos\psi_2 + c_2 \end{cases} \varphi \in [\varphi_1 + 2n_1\pi, \varphi_{max} \tag{10}$$

Where

$$\psi_1 = arctan\left|\frac{k_1-k_2}{1+k_1k_2}\right| \tag{11}$$

$$\psi_2 = arctan\left|\frac{k_3-k_4}{1+k_3k_4}\right| \tag{12}$$

Where (b_1, c_1) are the values of the horizontal and vertical coordinates of point C, (b_2, c_2) are the values of the horizontal and vertical coordinates of point D,ψ_1 is the tangent angle between S_1 and $S_{E''F''}$ at point C， ψ_2 is the tangent angle between $S_{E''F''}$ and S_3 at point D, k_1 is the slope of S_1 at point C, k_2 is the slope of $S_{E''F''}$ at point C, k_3 is the slope of $S_{E''F''}$ at point D, k_4 is the slope of S_3 at point D.

Based on the above baseline equation and combined with the normal equidistant method, a new type of variable cross-section scroll profile can be constructed, as shown in Figure 3 (Pengcheng et al., 2021). The dashed part in the figure is a constant cross-section scroll profile composed of a single base circle involute. It can be clearly seen that any constant cross-section scroll profile can be replaced by a newly constructed variable cross-section profile to reduce the number of circles of the profile, shorten the length of the radial leakage line, increase the compression ratio, and improve efficiency.

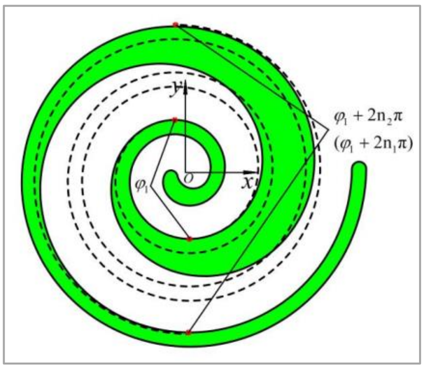

Figure 3: Variable cross-section scroll profile

3. Performance Indicators and Evaluation

The volumetric performance and mechanical performance of the profile directly affect the overall performance of the scroll compressor. To quantitatively measure the performance of the newly constructed variable cross-section scroll profile, a key indicator in mechanical performances, namely axial gas force and two important indicators in volumetric performances, namely compression ratio and radial leakage line length, have been introduced.

3.1 Axial Gas Force

In the working chamber of the working compressor, the gas force acting on the orbiting scroll along the main axis direction is called the axial gas force, represented by the symbol F_a. This force is the most important force acting on the orbiting scroll, and it is also one of the main drawbacks of the scroll compressor (Shusheng et al., 2019). Its effect will cause the orbiting and fixed scroll to detach from each other in the axial direction, leading to an increase in radial leakage. Therefore, the smaller the axial gas force acting on the orbiting scroll, the more beneficial it is to improve the mechanical performance of the scroll compressor. The calculation formula can be written as

$$F_a(\theta) = \begin{cases} \frac{1}{\square}\sum_{i=1}^{3} p_i(\theta)A_i(\theta) + p_s[A_4(0) - A_4(\theta)] \\ \qquad \theta \in [0, \theta^*) \\ \frac{1}{\square} p_3(\theta)A_3(\theta) + p_s[A_4(0) - A_4(\theta)] + \\ p_1(\theta)A_2(\theta) \\ \qquad \theta \in [\theta^*, 2\pi] \end{cases} \tag{13}$$

Where $p_1(\theta)$, $p_2(\theta)$, and $p_3(\theta)$ are the pressures of the corresponding working chamber, which can be calculated according to the following equation

$$p_i(\theta) = \begin{cases} p_s[\frac{A_4(0)}{A_i(\theta)}]^{\kappa} (i = 2,3) \\ p_s[\frac{A_4(0)}{A_2(\theta^*)}]^{\kappa} (i = 1) \end{cases} \tag{14}$$

Where p_s is the suction pressure, taking $p_s = 0.1013$Mpa. θ is the spindle angle, θ^* is the starting exhaust angle, κ is the isentropic index of the gas, taken as $\kappa = 1.21$. A_i is the cross-sectional area of the corresponding working chamber.

During the operation of the scroll compressor, the inner and outer wall profiles that make up the orbiting and fixed scroll mesh with each other to form pairs of closed crescent shaped working chambers, These chambers periodically change with the rotation of the spindle. as shown in Figure 4. They are sequentially referred to as the first compression chamber, the second compression chamber, the third compression chamber, and the suction chamber from the inside out.

According to the normal equidistant method to calculate the cross-sectional area of each working chamber, and the calculation process is as follows

The cross-sectional area of the suction chamber composed of the second and third base circle involutes can be given by

$$A_4(\theta) = 2R_{or}[L_s + R_g(\varphi\pi_{g_{max_{max}}} \tag{15}$$

Where

$$L_s = \int_{\varphi_1 + 2n_1\pi}^{\varphi_{max} - \theta} \sqrt{(x_3')^2 + (y_3')^2} d\varphi + \int_{\varphi_1 + 2n_2\pi}^{\varphi_{max} - 2\pi - \theta} \sqrt{(x_2')^2 + (y_2')^2} d\varphi \tag{16}$$

The cross-sectional area of the third compression chamber composed of the first and second base circle involutes can be obtained by

$$A_3(\theta) = 2R_{or}[L_c + R_g(\varphi\pi_g\pi_{max_{max}} \tag{17}$$

Where

$$L_c = \int_{\varphi_1}^{\varphi_{max} - 6\pi - \theta} \sqrt{(x_1')^2 + (y_1')^2} d\varphi + \int_{\varphi_1}^{\varphi_{max} - 4\pi - \theta} \sqrt{(x_2')^2 + (y_2')^2} d\varphi \tag{18}$$

When the working chamber is composed of the first base circle involute and a modified double arc, as shown in Figure 5, a second compression chamber can be formed.

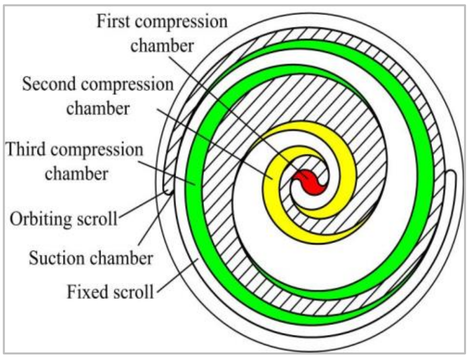

Figure 4: Schematic diagram of working chamber

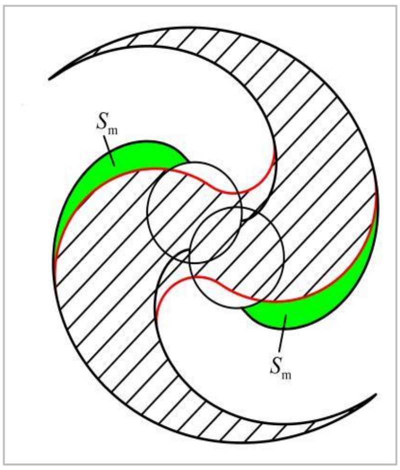

Figure 5: The second compression chamber

According to the geometric relationship, the cross-sectional area of the chamber can be expressed as:

$$A_2(\theta)=\frac{1}{3}a^2[(\theta+\frac{\pi}{2}-\partial)^3-(\theta-\frac{\pi}{2}+\partial)^3+(\phi+\pi+\partial)^3-(\phi+\pi-\partial)^3]-a^2(\pi-4\partial)-2S_m \tag{19}$$

Where

$$S_m=\frac{1}{6}a^2[(\phi+\pi+\partial)^3-(\phi+\partial)^3]+\frac{\pi}{2}a^2-\frac{\lambda}{2}(R_d{}^2-R_x{}^2) \tag{20}$$

Where R_{or} is the radius of rotation, ϕ is the corrected spanwise angle, ∂ is the angle of involute occurrence, λ is the center angle of the corrected arc, R_d is the corrected large arc radius, R_x is the corrected small arc radius.

When the working chamber is completely composed of modified double arcs, it can form the first compression chamber, its cross-sectional area can be obtained by

$$A_1(\theta)=(R_d{}^2-R_x{}^2)[\frac{\pi}{2}-\gamma-\theta-\sin(\frac{\pi}{2}-\gamma-\theta)] \tag{21}$$

Where γ is the correction angle.

3.2 Compression Ratio

The compression ratio is an important indicator for measuring the performance of scroll profiles. The higher the compression ratio, the better the volumetric performance of the profile. The compression ratio is defined as

$$\zeta=[A_4(0)/A_2(\theta^*)]^{\kappa} \tag{22}$$

3.3 Radial Leakage Line Length

The radial leakage of the scroll compressor not only reduces the gas delivery rate, but also increases the temperature inside the working chamber, resulting in greater leakage. Therefore, only by shortening the length of the radial leakage line can the leakage amount be effectively reduced, and its calculation formula can be represented as follows

$$L_x=\int_0^{\varphi_1}\sqrt{(x_1')^2+(y_1')^2}\mathrm{d}\varphi+\int_{\varphi_1}^{\varphi_1+2n_2\pi}\sqrt{(x_2')^2+(y_2')^2}\mathrm{d}\varphi+\int_{\varphi_1+2n_1\pi}^{\varphi_{max}}\sqrt{(x_3')^2+(y_3')^2}\mathrm{d}\varphi \tag{23}$$

As shown in Figure 6, it is a constant cross-section scroll profile composed of a single base circle involute, a variable cross-section scroll profile composed of base circle involute, higher-order curve as well as base circle involute, and a variable cross-section scroll profile composed of base circle involute, higher-order curve as well as arc.

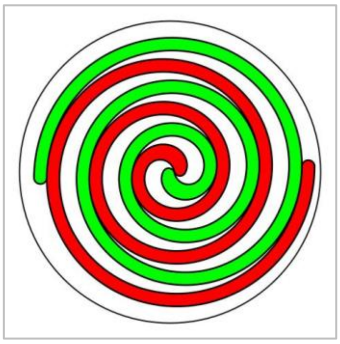

(a) Constant cross-section scroll profile

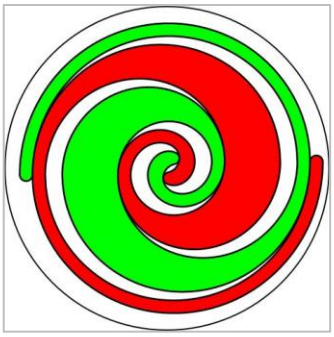

(b) Variable cross-section scroll profile composed of circle involutes and higher-order curve

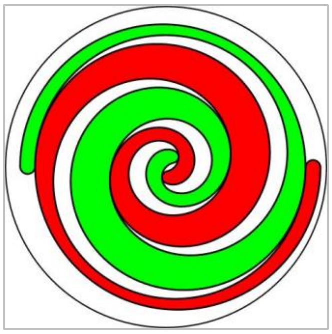

(c)Variable cross-section scroll profile composed of circle involute, higher-order curve and arc

Figure 6: Traditional scroll profiles

Under the same basic parameters, compare the newly constructed variable cross-section scroll profile with the three traditional scroll profiles mentioned above, and the results are shown in Table 1 and Figure 7.

From Table 1, it can be seen that compared with the traditional scroll profiles, the performance indicators examined by the newly constructed profile have significantly improved. Compared to the constant cross-section profile, the compression ratio of the newly constructed variable cross-section profile has increased by 28.62%, and the length of the radial leakage line has been shortened by 26.56%. Compared with the traditional variable cross-section profile composed of base circle involute, higher order curve, base circle involute and base circle involute, higher order curve and arc, the compression ratio of the newly constructed variable cross-section profile has been increased by 16.51% and 7.58%, respectively, and the length of the radial leakage line has been shortened by 16.37% and 14.23%, respectively. This quantitatively confirms that the new variable cross-section scroll profile is superior to the traditional constant cross-section profile and variable cross-section profile.

Table 1: Comparison of volumetric performances

Profile type (code name)	ζ	L_x / mm
constant cross-section profile (SP_1)	7.765	640
circle involutes-higher order curve variable cross-section profile (SP_2)	8.572	562
circle involute-higher order curve-arc variable cross-section profile (SP_3)	9.283	548
newly constructed variable cross-section profile (SP_4)	9.987	470
Δ / % (SP_4 relative to SP_1)	28.62	-26.56
Δ / % (SP_4 relative to SP_2)	16.51	-16.37
Δ / % (SP_4 relative to SP_3)	7.58	-14.23

As shown in Figure 7, from the magnitude of axial gas force, the newly constructed variable cross-section scroll profile has the smallest axial gas force; The axial gas force of the variable cross-section scroll profile composed of base circle involute, higher order curve, and base circle involute is the highest; The axial gas force of the other profiles is between these two. From this, it can be seen that traditional scroll profiles will cause the fixed and orbiting scroll to detach from each other due to excessive axial gas force, leading to increased leakage. The new scroll profile is more conducive to improving the overall performance of the compressor because of its smaller axial gas force. From the trend of changing, the variable cross-section scroll profile composed of base circle involute, higher order curve as well as base circle involute and base circle involute, higher order curve as well as arc introduce higher order curves, resulting in a larger fluctuation amplitude of axial gas force. Since the fact that both the constant cross-section profile and the newly constructed variable cross-section profile use base circle involutes, the axial gas force variation amplitude is relatively small, which also indicates that base circle involutes have stable performance characteristics.

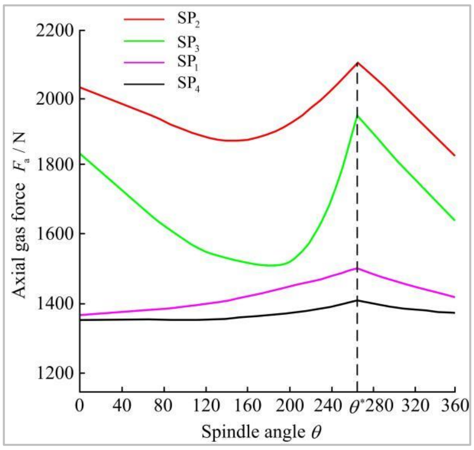

Figure 7: Axial gas force variation curves of different profiles

4. Conclusion

Based on the study of variable cross-section scroll profiles and combined with the stable performance and easy processing characteristics of base circle involutes, a theory of constructing variable cross-section scroll profiles using base circle involutes is proposed, and a new variable cross-section scroll profile is constructed using this theory. The newly constructed variable cross-section scroll profile not only breaks through the constraints of higher-order curves in its construction method, but also exhibits significant advantages in terms of volumetric and mechanical performances. Compared with the traditional constant cross-section profile as well as the variable cross-section profiles, the compression ratio is significantly increased, the radial leakage line length is shortened obviously, and the axial gas force is apparently reduced. It can be seen that the newly constructed variable cross-section profile helps to further improve the performance of scroll compressors and effectively promotes the application of variable cross-section scroll compressors in practice.

References

Ahmad, M., Marjan, M., Tracie, B., 2020. Compression chamber volume analysis for co-rotating scroll compressors. International Journal of Refrigeration, 112, Pp. 172-188.

Caisheng, H., Tao, L., 2019. Effect of profile parameters on tooth thickness for variable cross-section scroll compressor. Transactions of Beijing Institute of Technology, 39 (11), Pp. 1107-1112.

Cavazzini, G., Giacome, F., Ardizzon, G., 2020. CFD-based optimization of scroll compressor design and uncertainty quantification of the performance under geometrical variations. Energy, 209, Pp. 118382.

Diniz, M.C., Pereira, E., Deschamps, C.J., 2015. A lumped-parameter thermal model for scroll compressors including the solution for the temperature distribution along the scroll wraps. International Journal of Refrigeration, 53, Pp. 184-194.

Ivlev, V.I., Misyurin, S.Y., 2017. Calculated and experimental characteristics of a scroll machine operating in the air motor mode. Doklady Physics, 62 (1), Pp. 42-45.

Jiahao, W., Xia, S., Junye, S., Jiangpin, C., 2022. Profile design and leakage characteristics of scroll compressor with trapezoidal cross section. Journal of Refrigeration, 43 (02), Pp. 46-53.

Jianguo, Q., Zhenquan, L., 2009. Analysis and simulation of scroll compressor chamber's deformation. Journal of System Simulation, 21 (6), Pp. 1515-1517, 1525.

Licun, W., Shiliu, L., Yong, M., Xianming, Z., 2009. Dynamics of Jogging principle forscroll profiles of scroll compressor. Journal of Harbin Institute of Technology, 41 (7), Pp. 187-189.

Ling, F., Chunmei, J., Zhongchang, Q., Guoji, S., 2003. Correlation analysis of scroll compressor profile error sensitivityand radial mesh clearance. Chinese Journal of Mechanical Engineering, 39 (4), Pp. 151-154.

Pengcheng, Z., Bin, P., Jie, M., 2021. A variable thickness scroll machines composed of algebraic spiral. Journal of Huazhong University of Science and Technology (Natural Science Edition), 49 (5), Pp. 56-61.

Pereira, E.L., Deschamps, C.J., 2020. Numerical analysis and correlations for radial and tangential leakage of gas in scroll compressors. International Journal of Refrigeration, 2 (110), Pp. 239-247.

Qiu, K., Thomas, M., Douglas, M., 2018. Investigation of a scroll expander driven by compressed air andits potential applications to ORC. Applied Thermal Engineering, 135, Pp. 109-115.

Rak, J., Pietrowicz, S., 2020. Internal flow field and heat transfer investigation inside the working chamber of a scroll compressor. Energy, 202, Pp. 117700.

Shuai, Z., Jianhua, W., Che, W., Hua, Z., Zibo, Z., 2023. Study on a variable wall thickness profile ofelectric scroll compressor used for automobile airconditioner. Journal of Power and Energy, 237 (2), Pp. 294-307.

Shusheng, X., Renpu, J., W.U., Zhankuan, Z., Teng, P., Shuhao, 2019. Simulation analysis of stress and deformation of scrollplate of fuel cell air compressor under uniform load. Journal of Tongji University (Natural Science), 47 (S1), Pp. 146-153.

Zhen, L., Zheng, L., Dongsheng, X., Huawei, W., 2022. Unsteady characteristic and flow mechanism of ascroll compressor in small-scale compressed airenergy storage system. Journal of Energy Storage, 51, Pp. 104368.